Unblocking of stellar electron capture for neutron-rich $N = 50$ nuclei at finite temperature

Alan A. Dzhioev [1,*] K. Langanke,[2,3] G. Martínez-Pinedo,[2,3] A. I. Vdovin,[1] and Ch. Stoyanov[4]

[1]*Bogoliubov Laboratory of Theoretical Physics, JINR, 141980, Dubna, Russia*
[2]*GSI Helmholzzentrum für Schwerionenforschung, Planckstraße 1, 64291 Darmstadt, Germany*
[3]*Institut für Kernphysik (Theoriezentrum), Technische Universität Darmstadt, Schlossgartenstraße 2, 64289 Darmstadt, Germany*
[4]*Institute for Nuclear Research and Nuclear Energy, Bulgarian Academy of Sciences, 1784 Sofia, Bulgaria*

We have calculated electron-capture rates for neutron-rich $N = 50$ nuclei (^{78}Ni, ^{82}Ge, ^{86}Kr, ^{88}Sr) within the thermal quasiparticle random-phase approximation approach at temperatures $T = 0$, corresponding to capture on the ground state, and at $T = 10$ GK (0.86 MeV), which is a typical temperature at which the $N = 50$ nuclei are abundant during a supernova collapse. In agreement with recent experiments, we find no Gamow-Teller (GT$_+$) strength at low excitation energies, $E < 7$ MeV, caused by Pauli blocking induced by the $N = 50$ shell gap. At the astrophysically relevant temperatures, this Pauli blocking of the GT$_+$ strength is overcome by thermal excitations across the $Z = 40$ proton and $N = 50$ neutron shell gaps, leading to a sizable GT contribution to the electron capture. At the high densities, at which the $N = 50$ nuclei are important for stellar electron capture, forbidden transitions contribute noticeably to the capture rate. Our results indicate that the neutron-rich $N = 50$ nuclei do not serve as an obstacle of electron capture during supernova collapse.

I. INTRODUCTION

Electron captures on nuclei play an essential role during the collapse of a massive star leading to a type-II or core-collapse supernova [1–4]. It reduces the electron-to-baryon ratio Y_e and hence the pressure which the relativistic degenerate electron gas can stem against the gravitational collapse. As the neutrinos produced by the capture process can leave the star, carrying away energy, it is also an effective cooling mechanism, resulting in the fact that heavy nuclei survive during the collapse [1]. The temperature in the collapsing core is sufficiently high that nuclei exist in nuclear statistical equilibrium (NSE) [5]. However, due to the decrease of Y_e by continuous electron capture, the abundance distribution of nuclei is shifted to more neutron-rich and heavier nuclei during the collapse.

Due to the electron energies involved, electron captures are dominated by allowed Gamow-Teller (GT$_+$) transitions (in which a proton is changed to a neutron) at the early stage of the collapse. However, forbidden transitions become increasingly important with growing electron energies and contribute significantly to the capture rates in the later collapse phases [6,7]. For core densities, $\rho \lesssim 10^{10}$ g cm^{-3} and the respective temperatures the core composition of nuclei is given by pf shell nuclei in the iron-nickel mass region. For these nuclei, electron capture rates can be calculated on the basis of large-scale shell-model diagonalization calculations [8–10]. The calculations reproduce the GT$_+$ distributions

experimentally determined by charge-exchange reactions [11,12] quite well [13–15]. These rates are significantly smaller than the pioneering rates by Fuller *et al.* [16], resulting in a slower deleptonization in the early collapse phase [17,18].

As noted by Fuller [19], the continuous shift of the NSE abundance distribution to heavier and more neutron-rich nuclei can lead to a potential blocking of the GT$_+$ strength, once nuclei with proton numbers $Z < 40$ and neutron numbers $N > 40$ dominate the core composition. For such nuclei, GT$_+$ transitions are completely Pauli blocked within the simple independent-particle model. Based on this observation, Bruenn derived stellar capture rates which predicted vanishing capture rates for nuclei with $N > 38$ [20]. These capture rates have been the standard in supernova simulations for many years and led to the conclusion that electron capture proceeds on free protons in the advanced collapse phases (see, e.g., Ref. [2]). Cooperstein and Wambach pointed out that the Pauli blocking might be overcome by thermal excitations, but which would only happen at core densities in excess of 10^{11} g cm^{-3} [6]. However, the $N = 40$ shell closure is overcome by cross-shell correlations which move neutrons and protons into the $g_{9/2}$ orbital and hence open up GT$_+$ transitions. Experimentally this is observed for ^{76}Se ($Z = 34$, $N = 42$) which has a nonvanishing GT$_+$ strength distribution (required for the double-beta decay of ^{76}Ge [12,21]), made possible by a sizable neutron-hole structure in the pf shell as determined from transfer reactions [22]. The experimental GT$_+$ distribution is well described by shell-model diagonalization studies [23] confirming that cross-shell correlations require multiparticle-multihole correlations [24,25]. For stellar electron-capture rates, these correlations have been considered within a hybrid

model, in which nuclear partial occupation numbers have been calculated within the shell-model Monte Carlo approach [26,27], which allows us to determine thermally averaged nuclear properties at finite temperatures considering correlations in unprecedentedly large model spaces (here the full pf-gds shells). The partial occupation numbers served as input to a random-phase approximation (RPA) calculation of the stellar electron-capture rates [28]. Incorporated into supernova simulations these rates had noticeable effects on the supernova dynamics [4,29] and showed that electron capture is dominated by nuclei during the entire collapse.

Sullivan *et al.* [30,31] have pointed out that the $N = 50$ shell gap at the neutron $g_{9/2}$ shell closure could act as a severe obstacle for stellar electron capture, in particular for nuclei with proton number $Z < 40$ because they are frequently encountered at core densities before neutrino trapping (at a few 10^{11} g cm^{-3}). The argument is based on the observation that Pauli unblocking by neutron holes in the pf shell is strongly hindered by the gap, and that proton excitations into the $g_{9/2}$ orbital would mainly lead to GT$_+$ transitions into the neutron $g_{7/2}$ orbital residing at modest excitation energies in the daughter and hence will not noticeably contribute to the electron-capture rate. Sullivan and collaborators supported their argument by studies with parametrized stellar electron-capture rates which indicated the $N = 50$ nuclei as an obstacle to the supernova dynamics [30,31]. Motivated by these studies, Zegers *et al.* measured the GT$_+$ strength distribution in two relevant nuclei, ^{86}Kr ($Z = 36$, $N = 50$) [32] and ^{88}Sr ($Z = 38$, $N = 50$) [33]. Both distributions indeed show no GT$_+$ strength at low energies. These authors then used the experimental GT$_+$ distributions for the nuclear ground states to determine stellar electron-capture rates. Such a procedure would be valid if the Brink-Axel hypothesis holds, i.e., the GT$_+$ distribution on all excited states is the same as for the ground state.

As we show in the following, this assumption is inappropriate. At first, in the stellar core the capture occurs at finite temperatures of about $T = 1$ MeV. Adopting the simple Fermi gas ansatz, this temperature translates into excitation energies ($E^* \approx AT^2/8$) of about 10 MeV, which is larger than the shell gaps at $N = 50$ and $Z = 40$. Hence, the capture occurs on a thermal nuclear ensemble which includes excited states with proton particles in the $g_{9/2}$ orbital and neutron holes in the pf and $g_{9/2}$ orbitals. These correlations unblock GT$_+$ transitions at low energies or can even lead to nuclear deexcitation where nuclear excitation energy is transferred to the leptons. We note that a sizable unblocking of the GT$_+$ strength by correlations and thermal excitations was found in the hybrid SMMC/RPA calculations, exemplified for ^{89}Br in Ref. [28], and for $^{76-80}$Ge, ^{78}Ni based on the thermal quasiparticle random-phase approximation (TQRPA) approach [34,35]. These studies also showed that forbidden transitions, which are not hindered by the shell gap, contribute sizably to the stellar capture rates at the conditions which are relevant for $N = 50$ nuclei.

In this paper we extend the TQRPA study of Dzhioev and collaborators to a chain of $N = 50$ nuclei, including the two nuclei (^{86}Kr and ^{88}Sr) for which experimental GT$_+$ distributions have been measured for the ground states. The

TQRPA consistently describes thermal properties of nuclei at finite temperatures considering 2p-2h correlations induced by pairing and a residual interaction. In the limit of vanishing temperatures, it reduces to the QRPA model. Our focus is here on the aspect how the correlations unblock the GT$_+$ strength at finite temperature and which consequences this unblocking has on the stellar electron-capture rate. We also calculate the forbidden contributions to the rate. Our main result is that the capture rate for $N = 50$ nuclei at the finite temperatures, which are relevant in a supernova collapse, is much larger than estimated on the basis of the GT$_+$ ground-state distributions.

We should mention several papers where different finite-temperature RPA models based on Skyrme and relativistic energy density functionals have been used to calculate stellar electron-capture (EC) rates [36–38]. The TQRPA approach differs from those of Refs. [36–38] primarily by thermodynamically consistent consideration of thermal effects. It was shown in Ref. [39] that exoergic transitions from thermally excited states appear within the TQRPA and for EC on ^{56}Fe they remove the reaction threshold and enhance the low-energy cross section. In contrast, no such transitions appear within the finite-temperature RPA models. As a result, calculations in Refs. [36–38] predict that EC cross sections drop rapidly to zero as the electron energy falls below some threshold value.

Our paper is organized as follows: In the next section we give a brief outline of the TQRPA method which we have used in our calculations. A comprehensive description of the thermal QRPA approach is given in Refs. [34,35]. In Sec. III we discuss the results of our calculations. In Sec. IV we provide the concluding remarks.

II. ELECTRON CAPTURE IN THE THERMAL QUASIPARTICLE RANDOM-PHASE APPROXIMATION APPROACH

Due to the high temperature in the interior of massive stars, there is a finite probability of occupation of nuclear excited states in the stellar environment. We account for this by defining a thermal-averaged cross section for capture of an electron with energy ε_e on a particular nucleus

$$\sigma(\varepsilon_e, T) = \sum_{if} p_i(T)\sigma_{if}(\varepsilon_e). \tag{1}$$

Here, $p_i(T)$ is the Boltzmann population factor for a parent state i at temperature T, and $\sigma_{if}(\varepsilon_e)$ is the cross section for capture of an electron from the state i to a state f in the daughter nucleus. Then, the stellar electron-capture rate $\lambda(T)$ at finite temperature is obtained by folding the thermal-averaged cross section $\sigma(\varepsilon_e, T)$ with the distribution of electrons,

$$\lambda(T) = \frac{1}{\pi^2\hbar^3} \int_{m_ec^2}^{\infty} \sigma(\varepsilon_e, T)p_e^2 f(\varepsilon_e)d\varepsilon_e, \tag{2}$$

where $p_e = (\varepsilon_e^2 - m_e^2c^4)^{1/2}/c$ is the momentum of the incoming electron. Under conditions encountered in the collapsing core of a supernova, electrons obey a Fermi-Dirac distribution $f(\varepsilon_e)$ with temperature T and electron chemical potential μ_e which depend on the baryon density ρ and the electron-to-baryon ratio Y_e.

The nuclei of interest in this study are expected to contribute to the stellar electron-capture rates for temperatures $T \approx 0.5$–1.5 MeV. At such high temperatures an explicit state-by-state evaluation of the sums in Eq. (1) is impossible with current nuclear models. As was shown in Ref. [35], within a statistical description, the thermal-averaged cross section can be expressed through the temperature-dependent spectral functions for the various momentum-dependent multipole operators derived in Refs. [40,41].

Although our calculations also consider forbidden transitions, we will give special emphasis to the GT_+ contribution for the nuclear structure reasons outlined above. Neglecting momentum transfer, the thermal-averaged cross section for GT operators reduces to

$$\sigma_{GT}(\varepsilon_e, T) = \frac{G_F^2 V_{ud}^2}{2\pi \hbar^4 c^3 v_e} F(Z, \varepsilon_e)$$
$$\times \int_{-\infty}^{E_e} (\varepsilon_e - E)^2 S_{GT}(E, T) dE, \qquad (3)$$

where $S_{GT}(E, T)$ is the temperature-dependent strength function for the Gamow-Teller operator

$$S_{GT}(E, T) = \sum_{if} p_i(T) \frac{|\langle f \| g_A \sigma t_+ \| i \rangle|^2}{2J_i + 1} \delta(E - E_{if}). \qquad (4)$$

In the above equations G_F is the weak-interaction coupling constant, $g_A = -1.27$ is the axial-vector coupling constant, and V_{ud} is the up-down element in the Cabibbo-Kobayashi-Maskawa quark mixing matrix. The Fermi function $F(Z, \varepsilon_e)$ corrects the cross section for the distortion of the electron wave function by the Coulomb field of the nucleus [8] and v_e is the electron velocity. The transition energy between initial and final states is given by $E_{if} = Q + E_f - E_i$, where E_i and E_f are the excitation energies of the parent and daughter nuclei, and $Q = M_f - M_i$ is the ground-state reaction threshold. At $T \neq 0$, due to transitions from thermally excited states, the strength function $S_{GT}(E, T)$ is defined for both $E > Q$ and $E < Q$ domains.

To compute the temperature-dependent spectral functions we apply the TQRPA framework [34,35,39,42,43], which is a technique based on the proton-neutron QRPA extended to finite temperature by the thermofield dynamics formalism (TFD) [44,45]. The TFD doubles the degrees of freedom of the quantum system by introducing a fictitious tilde Hamiltonian $\widetilde{H}$ and uses an extended Hilbert space of the direct product of the Hilbert spaces of the physical and fictitious systems. The central concept in TFD is the thermal vacuum $|0(T)\rangle$, a pure state in the extended Hilbert space, which corresponds to the thermal equilibrium, a mixed state in the original Hilbert space of the system. The time-translation operator in the extended Hilbert space is a so-called thermal Hamiltonian $\mathcal{H} = H - \widetilde{H}$. The temperature-dependent strength function is expressed by the transition matrix elements from the thermal vacuum to eigenstates of the thermal Hamiltonian ($\mathcal{H}|Q_i\rangle = \omega_i |Q_i\rangle$):

$$S_A(E, T) = \sum_i |\langle Q_i | \hat{A} | 0(T) \rangle|^2 \delta(E - \omega_i - \delta_{np}). \qquad (5)$$

Here $\delta_{np} = \Delta\lambda_{np} + \Delta M_{np}$, and $\Delta\lambda_{np} = \lambda_n - \lambda_p$ is the difference between neutron and proton chemical potentials in the nucleus, and $\Delta M_{np} = 1.293$ MeV is the neutron-proton mass splitting. Note that eigenvalues of the thermal Hamiltonian, ω_i, take both positive and negative values. The latter contribute to the strength function only at $T \neq 0$.

Within the TQRPA, the thermal Hamiltonian is diagonalized in terms of thermal phonon operators, which are constructed as a linear superposition of the creation and annihilation operators for proton-neutron thermal quasiparticle pairs: $\beta_p^\dagger \beta_n^\dagger$, $\beta_p^\dagger \widetilde{\beta}_n^\dagger$, $\widetilde{\beta}_p^\dagger \beta_n^\dagger$, $\widetilde{\beta}_p^\dagger \widetilde{\beta}_n^\dagger$, and their Hermitian conjugates. Correspondingly thermal quasiparticles are connected with Bogoliubov quasiparticles by the so-called thermal Bogoliubov transformation which mixes nontilde and tilde operators. It can be shown [34] that the creation of a negative-energy thermal tilde quasiparticle corresponds to annihilation of a thermally excited Bogoliubov quasiparticle. Because of single-particle transitions involving annihilation of thermally excited Bogoliubov quasiparticles, the phonon spectrum at finite temperature contains states at negative and low energies which do not exist at zero temperature and which correspond to thermally unblocked transitions of excited nuclear states. In the zero-temperature limit, the thermal phonons reduce to the QRPA ones constructed of Bogoliubov quasiparticle pairs $\alpha_p^\dagger \alpha_p^\dagger$ and $\alpha_p \alpha_n$.

To analyze unblocking effects for EC in neutron-rich nuclei with $N = 50$, we perform Skyrme-TQRPA calculations in ^{78}Ni, ^{82}Ge, ^{86}Kr, and ^{88}Sr. To explore the possible variations among parametrizations, we have chosen two different Skyrme parametrizations with sufficiently different properties, SkM* [46] and SkO′ [47]. We solve Skyrme-Hartree-Fock equations assuming spherical symmetry and neglecting thermal effects on the mean field. To take into account pairing correlations between like particles we employ the BCS pairing interaction. The pairing strength parameters are fixed to reproduce the odd-even mass difference. Due to magic neutron number $N = 50$, there is no neutron pairing. Moreover, there is no proton pairing in ^{78}Ni and ^{88}Sr, while proton pairing gaps in ^{82}Ge and ^{86}Kr at $T = 0$ are $\Delta_p = 1.22$ and 1.28 MeV, respectively. For very neutron-rich nuclei considered in the present work the difference between the neutron and proton chemical potentials is large enough to disregard isoscalar proton-neutron pairing in the mean field.

At $T \neq 0$ the pairing gap and the chemical potentials $\lambda_{n,p}$ are found from finite-temperature BCS equations [34]. The numerical solution of these equations yields vanishing pairing correlations above a critical temperature $T_{cr} \approx 0.5\Delta$ [48,49]. In the TQRPA calculations, we use the Landau-Migdal force as the residual particle-hole interaction with the parameters derived from the Skyrme interaction [50,51]. We neglect the proton-neutron pairing in the residual interaction. It is well known that the low-lying GT strength responsible for beta decay [52] and double-beta decay [53] is sensitive to the isoscalar proton-neutron pairing interaction. However, the nuclei we consider dominate the nuclear composition of the collapsing core at high enough temperatures ($T > T_{cr}$), when particle-particle correlations vanish and the residual proton-neutron pairing interaction does not affect the strength distributions.
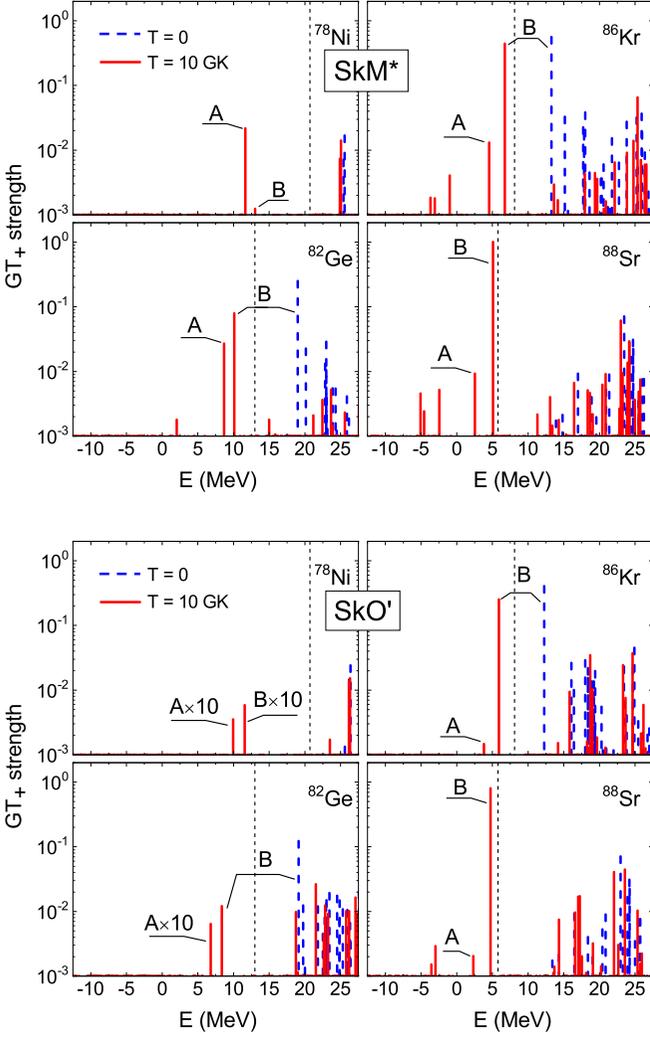
FIG. 1. Strength distributions of GT$_+$ transitions in ^{78}Ni, ^{82}Ge, ^{86}Kr, and ^{88}Sr at $T = 0$ and $T = 10$ GK (0.86 MeV). The dashed vertical lines indicate the ground-state thresholds $Q = M_f - M_i$: $Q(^{78}$Ni$) = 20.7$ MeV, $Q(^{82}$Ge$) = 13.0$ MeV, $Q(^{86}$Kr$) = 8.1$ MeV, and $Q(^{88}$Sr$) = 5.8$ MeV [54]. A and B label specific GT$_+$ transitions: $A \equiv f_{7/2}^p \to f_{5/2}^n$, $B \equiv g_{9/2}^p \to g_{7/2}^n$. The notations $A \times 10$ and $B \times 10$ mean that the respective peaks are scaled by a factor of 10 for demonstration purposes.

III. RESULTS AND DISCUSSION

In this section we report about TQRPA calculations for neutron-rich $N = 50$ nuclei performed at temperatures $T = 0$ and at $T = 10$ GK (0.86 MeV), which is a typical temperature at which these nuclei are abundant in collapsing supernova cores. Our main attention is laid upon the GT$_+$ response and its unblocking at finite temperatures, which is particularly important for the electron-capture rates on these nuclei under supernova conditions. Finally we supplement the GT part of the electron-capture rate by the contributions of the other multipoles.

Figure 1 shows our GT$_+$ response at $T = 0$ calculated with the Skyrme interaction SKM*. The results obtained with SkO′ are qualitatively similar. As GT$_+$ transitions are

completely blocked for nuclei with $Z < 40$ and $N > 50$, the calculated transitions are due to nuclear correlations induced by the Skyrme and the pairing forces. In our calculations the main unblocking mechanism in the ground states is due to the excitations of protons into the $g_{9/2}$ orbital, enabling GT$_+$ transitions into the $g_{7/2}$ neutron orbitals. However, these transitions reside at relatively modest excitation energies, resulting in the fact that there is no GT strength at low excitation energies for the ground-state distribution. This observation is in agreement with the measured GT$_+$ strengths for ^{86}Kr and ^{88}Sr, which both find no strength at low energies $E < 7$ MeV [32,33]. We note that the correlations across the $Z = 40$ and $N = 50$ shell gaps open up other possible GT$_+$ transitions; for example, between $f_{7/2}$ proton and $f_{5/2}$ neutron orbitals. But these transitions are small compared with $g_{9/2}^p \to g_{7/2}^n$ and reside at slightly higher excitation energies. We note that the $g_{9/2}^p \to g_{9/2}^n$ transition, which corresponds to rather small excitation energies and would be important for electron capture, requires the excitations of protons and neutrons across the shell gaps and hence is doubly suppressed in our model. Hence we do not find any relevant strength for this transition.

The ground-state ($T = 0$) GT$_+$ strength for the $g_{9/2}^p \to g_{7/2}^n$ transition (and for the other transitions) is noticeably larger for ^{82}Ge and ^{86}Kr than for ^{78}Ni and ^{88}Sr. This is related to the fact that proton pairing is absent in the latter two nuclei and nonvanishing GT$_+$ strength in ^{78}Ni and ^{88}Sr appears only at relatively high energies due to the admixture of $2\hbar\omega$ correlations. For ^{82}Ge and ^{86}Kr, configuration mixing is induced by the pairing interaction which mixes 0p0h and 2p2h configurations. For ^{82}Ge and ^{86}Kr, our BCS-SkM* calculations predict the occupation numbers $\langle n \rangle = 0.2$ and 0.4 protons in the $g_{9/2}^p$ orbital, respectively, thus making possible the $g_{9/2}^p \to g_{7/2}^n$ transition. The larger occupation number for ^{86}Kr reflects itself in the larger strength of the $g_{9/2}^p \to g_{7/2}^n$ transition, as seen in Fig. 1. At $T = 0$, this transition corresponds to the excitation of the $\alpha_{g_{9/2}^p}^\dagger \alpha_{g_{7/2}^n}^\dagger$ configuration above the ground state. The respective transition strength is proportional to the BCS amplitude $v_{g_{9/2}^p}^2$, while the transition energy is determined the sum of quasiparticle energies $\varepsilon_{g_{7/2}^n} + \varepsilon_{g_{9/2}^p} + \delta_{np}$.

At finite temperature the thermally averaged GT$_+$ strength is arising from an ensemble of excited nuclear states, where the centroid and the width of the ensemble increases with growing temperature. At the temperature of about $T = 1$ MeV, at which the neutron-rich $N = 50$ nuclei are expected to contribute to the stellar electron-capture rate, the structure of these states involves a larger occupation of particle orbitals above those occupied in the ground state, leaving at the time holes in orbitals occupied at $T = 0$. This mechanism thermally unblocks GT$_+$ transitions; for example, the $g_{9/2}^p \to g_{7/2}^n$ and $f_{7/2}^p \to f_{5/2}^n$ transitions, which in our TQRPA formalism are accompanied by annihilation of thermally excited particle and hole states. The resulting configurations above the thermal vacuum are $\widetilde{\beta}_{g_{9/2}^p}^\dagger \beta_{g_{7/2}^n}^\dagger$, $\beta_{f_{7/2}^p}^\dagger \widetilde{\beta}_{f_{5/2}^n}^\dagger$, while the transition strengths are proportional to $y_{g_{9/2}^p}^2 (1 - y_{g_{7/2}^n}^2)$, $(1 - y_{f_{7/2}^p}^2) y_{f_{5/2}^n}^2$. Here $y_j^2 = [1 + \exp(-\varepsilon_j / T)]^{-1}$ is the thermal occupation factor for a

single-particle state j. Within the TFD approach this factor stems from the thermal Bogoliubov transformation. We stress that the energies of the thermally unblocked transitions are $\varepsilon_{g_{7/2}^n} - \varepsilon_{g_{9/2}^p} + \delta_{np}$, $\varepsilon_{f_{7/2}^p} - \varepsilon_{f_{5/2}^n} + \delta_{np}$, which differs from the respective transition energies at $T = 0$ by the minus signs which correspond to annihilation of thermally excited states. Our calculated finite-temperature GT$_+$ strengths are shown in Fig. 1 together with the ground-state distributions for comparison. For all considered nuclei, thermally unblocked GT$_+$ transitions are located below the ground-state threshold Q, including the strength due to the dominant $g_{9/2}^p \rightarrow g_{7/2}^n$ and $f_{7/2}^p \rightarrow f_{5/2}^n$ transitions. This appearance of low-lying strength will have important consequences for the stellar electron-capture rates at finite temperatures. Moreover, for ^{86}Kr and ^{88}Sr we observe some thermally unblocked GT$_+$ strengths even at negative energies, which correspond to transitions from thermally excited states in the parent nucleus that are at higher energies than the final states in the daughter nucleus. Due to negative-energy transitions, nuclear excitation energy is transferred to the outgoing neutrinos.

Except for ^{78}Ni, the largest GT$_+$ strength resides in peaks which correspond mainly to $g_{9/2}^p \rightarrow g_{7/2}^n$ transitions. Its strength increases from ^{82}Ge to ^{88}Sr, related to the number of protons in the pf shell available for thermal excitations into the $g_{9/2}$ orbital. We also note that pairing correlations vanish with temperature and are already strongly diminished at $T = 10$ GK. As a consequence the noticeable peaks seen in the ground-state GT$_+$ distributions for ^{82}Ge and ^{86}Kr are suppressed in the TQRPA calculation at $T = 10$ GK. Referring to Fig. 1, at $T = 10$ GK the total GT$_+$ strength in ^{82}Ge and ^{86}Kr appears to be somewhat smaller than that at $T = 0$. The origin of nonmonotonic temperature dependence of the total GT$_+$ strength in neutron-rich nuclei is discussed in Ref. [34]. In particular it is shown that the total strength reaches a minimum value in the vicinity of the critical temperature $T \approx 0.5\Delta$, i.e., when pairing correlations vanish, but thermal effects are not yet sufficiently strong to occupy the $1g_{9/2}$ proton orbit and unblock the $1f_{5/2}$ neutron orbit. Note however, that the Ikeda sum rule is fulfilled within the TQRPA [43].

Figure 1 reveals that the strength of thermally unblocked $f_{7/2}^p \rightarrow f_{5/2}^n$ transitions depends rather noticeably on the Skyrme parametrization but varies only moderately among the different nuclei. In contrast, the peak related to the thermally unblocked $g_{9/2}^p \rightarrow g_{7/2}^n$ transition increases by almost three orders of magnitude between ^{78}Ni and ^{88}Sr, but it is rather insensitive to the choice of the Skyrme parametrization. To gain insight into this observation we plot in Fig. 2 the single-particle energies E_j for the particle ($g_{9/2}^p$, $g_{7/2}^n$) and hole ($f_{7/2}^p$, $f_{5/2}^n$) orbitals relative to the chemical potentials $\lambda_{n,p}$ at $T = 10$ GK, as calculated for the two Skyrme interactions. Note that for $T > T_{\mathrm{cr}}$ the quasiparticle energy is given by $\varepsilon_j = |E_j - \lambda|$. Hence $|E_j - \lambda|$ determines the occupation probabilities y_j^2 of the hole (particle) orbitals. For $T = 10$ GK, the proton orbital $f_{7/2}^p$ remains almost occupied (i.e., $1 - y_{f_{7/2}^p}^2 \approx 1$) and the strength of the $f_{7/2}^p \rightarrow f_{5/2}^n$ transition mainly depends on the number of thermally excited vacancies in the neutron orbital $f_{5/2}^n$. Figure 2 shows that the Skyrme
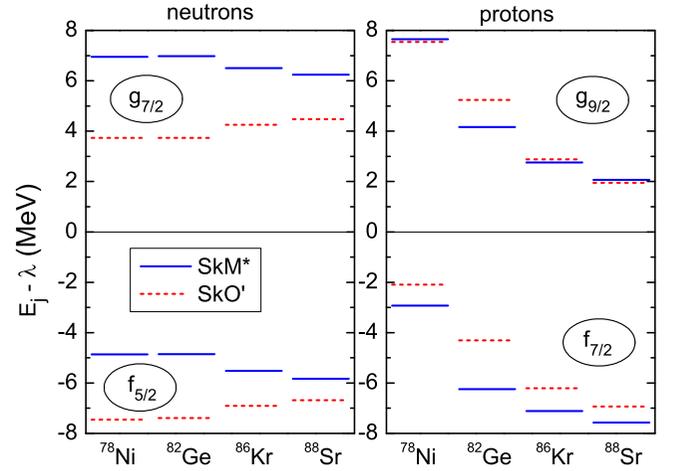

FIG. 2. Neutron ($f_{5/2}$, $g_{7/2}$) and proton ($f_{7/2}$, $g_{9/2}$) single-particle energies E_j relative to the chemical potentials $\lambda_{n,p}$ for $T = 10$ GK. The respective quasiparticle energies are given by $\varepsilon_j = |E_j - \lambda|$.

interaction SkO′ predicts a larger quasiparticle energy $\varepsilon_{f_{5/2}^n} = |E_{f_{5/2}^n} - \lambda_n|$ than the SkM* interaction. However, $E_{f_{5/2}^n} - \lambda_n$ does not change significantly with increasing proton number. As a consequence, the occupation factors $y_{f_{5/2}^n}^2$ obtained with the SkM* force are larger than those calculated with the SkO′ Skyrme interaction, but they do not vary much between the different nuclei. For the $g_{9/2}^p \rightarrow g_{7/2}^n$ transition, the thermally unblocked strength is mainly determined by the occupation of the $g_{9/2}^p$ orbital. Referring to Fig. 2, the quasiparticle energy $\varepsilon_{g_{9/2}^p} = E_{g_{9/2}^p} - \lambda_p$ reduces by a factor of four between ^{78}Ni and ^{88}Sr. This reduction increases the occupation factor $y_{g_{9/2}^p}^2$ and hence the transition strength by almost three orders of magnitude. Both Skyrme parametrizations predict rather similar values for $E_{g_{9/2}^p} - \lambda_p$.

The thermal unblocking of GT$_+$ transitions in the neutron-rich $N = 50$ nuclei reflects itself strongly in the GT contributions to the electron-capture cross sections. In Fig. 3 we plot thermal-averaged electron-capture cross sections at $T = 10$ GK and at $T = 20$ GK as a function of the incident electron energy ε_e in comparison with the ground-state ($T = 0$) results. In our calculations of the cross sections (and rates) we account for the quenching of the GT strength by the reduction of the axial-vector coupling constant g_A. In the context of shell-model calculations that really test individual GT transitions the quenching factor has been determined to be 0.74 for pf-shell nuclei [55,56]. With the same quenching factor, as shown in Ref. [34], the experimental GT$_+$ strength in pf-shell nuclei can be reproduced by the QRPA calculations. For all nuclei and for both interactions we observe a similar overall evolution of the cross sections with increasing temperature, reflecting the temperature dependence of the GT$_+$ strength distributions as discussed above. For all nuclei, the ground-state GT$_+$ distributions have no strength at low energies, representing a threshold for electron captures. Hence the $T = 0$ cross sections vanish at small electron energies. Once the capture threshold is overcome, the cross sections increase with electron energies, where the energy dependence is mainly
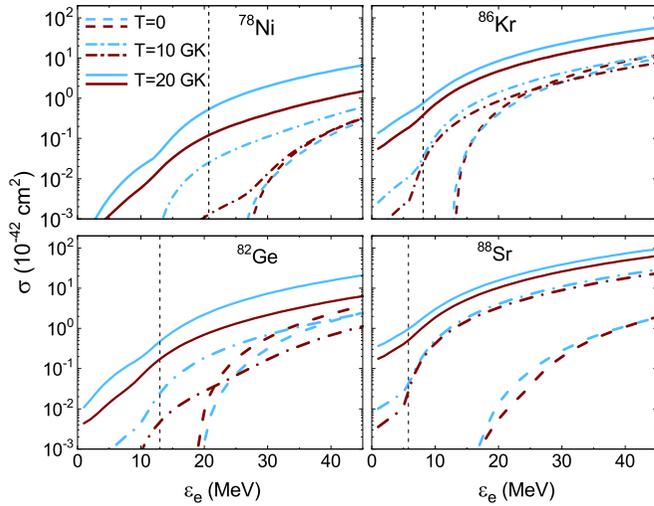
FIG. 3. Electron-capture cross sections for ^{78}Ni, ^{82}Ge, ^{86}Kr, and ^{88}Sr at $T = 0,\ 10,\ 20$ GK. The blue (light gray) and brown (dark gray) curves represent results obtained with the SkM* and SkO$'$ interactions, respectively. Like in Fig. 1, the dashed vertical lines indicate the ground-state thresholds $Q = M_f - M_i$.

dictated by phase space. With increasing temperatures, GT$_+$ strength is shifted towards lower energies (see Fig. 1), reducing the gap which has to be overcome or even removing it completely if strength is shifted to negative energies due to downscattering transitions (see discussion above). For the nuclei studied here, a gap exists in ^{78}Ni, even at $T = 20$ GK. For the other nuclei, the gap has vanished at this temperature as the reaction threshold completely disappears due to the contribution of GT$_+$ strength at negative energies.

The detailed energy dependence of the GT$_+$ strength is decisive at low electron energies, but becomes less relevant with increasing energy, where, however, the total strength matters [7]. In the two cases with proton pairing (^{82}Ge, ^{86}Kr) there is noticeable strength at moderate energies in our model calculations for $T = 0$ and the total strength is somewhat larger for the ground-state distribution than at $T = 10$ GK (see our discussion above). As a consequence the capture cross sections at high electron energies is slightly larger than at $T = 10$ GK. This phenomenon does not occur for ^{78}Ni and ^{88}Sr, where no proton pairing effects exist to create cross-shell correlations and hence the total ground-state strength is small. Relatedly, the increase of the cross sections with temperature is largest for these two nuclei. We also note that the differences in cross sections for the various nuclei become smaller with increasing electron energies, as had already been observed and explained in Refs. [7,34]. At the finite temperatures we have studied here, the cross sections at high energies increase with number of protons as the promotion of protons in the $g_{9/2}$ orbital is the main unblocking mechanism. Comparing the results obtained with the SkM* and SkO$'$ forces we conclude that the most essential differences in the cross sections exist in more neutron-rich nuclei at low temperatures and they reflect the differences in the GT$_+$ strength distributions discussed above.

Figure 4 shows electron-capture rates for ^{78}Ni, ^{82}Ge, ^{86}Kr, and ^{88}Sr at temperature 10 GK and for densities of
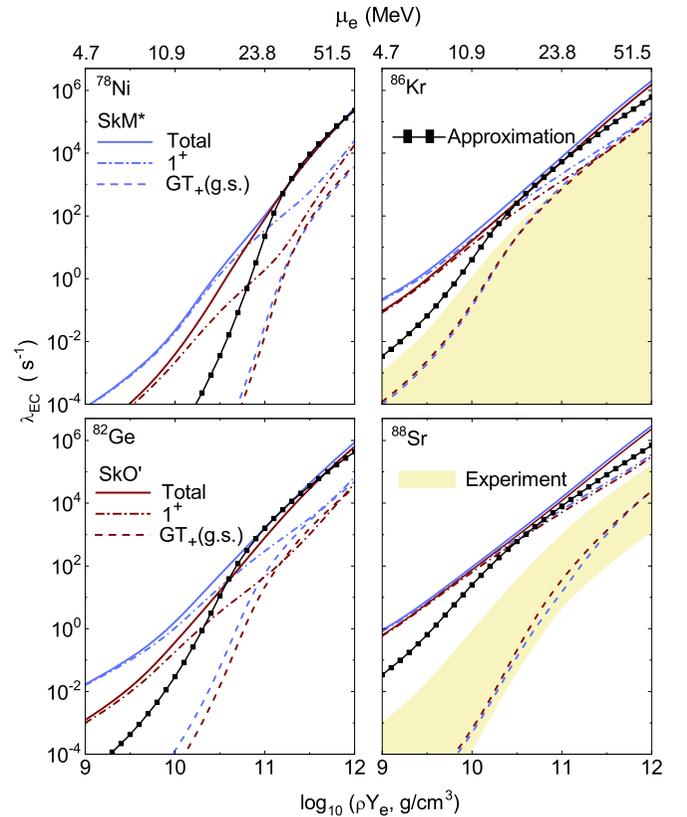

FIG. 4. Electron-capture rates calculated at $T = 10$ GK (0.86 MeV) as a function of density. The upper axis indicates the corresponding electron chemical potentials μ_e. The blue (light gray) and brown (dark gray) lines are based on the Skyrme-TQRPA calculations with the SkM* and SkO$'$ interactions, respectively. The total rates (full lines) include the contribution of allowed (0^+, 1^+) and first-forbidden (0^-, 1^-, 2^-) transitions. The dashed-dotted lines (labeled 1^+) represent the unblocked GT$_+$ contributions to the rates. The rates, indicated by dashed lines, have been calculated from the ground-state GT$_+$ distribution. The shaded bands represent the results based on the experimental GT$_+$ data [32,33]. The labeled lines represent the rates calculated according to the parametrization (6).

relevance for the collapse phase of core-collapse supernova.[1] Our rates are obtained by integrating the thermal-averaged cross sections following Eq. (2). In our rate calculations we have considered spectral functions for the allowed (0^+, 1^+) and first-forbidden (0^-, 1^-, 2^-) momentum-dependent multipole operators derived in Refs. [40,41]. To demonstrate the relevance of thermal unblocking and of multipoles other than Gamow-Teller, the figure also exhibits EC rates calculated from the ground-state and finite-temperature GT$_+$ distributions. For comparison we also show the capture rates for ^{86}Kr and ^{88}Sr derived from the experimental Gamow-Teller data [32,33]. The shaded bands are due to the experimental uncertainty in the GT$_+$ strength.

---

[1] For example, the core temperatures are in the range 10–14 GK for densities ρY_e between 2.4×10^{10} g and 2.3×10^{11} g cm^{-3} for a $15 M_\odot$ star due to Table 1 in Ref. [7].

TABLE I. Relative contribution, $\lambda_{EC}^{ff}/\lambda_{EC}$, of first forbidden transitions to the electron-capture rates at $T = 10$ GK and selected densities ρY_e (in g cm^{-3}). The results are obtained with the SkM* (SkO′) Skyrme interaction.

$\log_{10}(\rho Y_e) =$	9	10	11	12
^{78}Ni	0.04(0.17)	0.14(0.44)	0.66(0.97)	0.91(0.93)
^{82}Ge	0.07(0.20)	0.37(0.51)	0.82(0.94)	0.92(0.93)
^{86}Kr	0.09(0.09)	0.27(0.25)	0.71(0.75)	0.90(0.91)
^{88}Sr	0.08(0.06)	0.18(0.16)	0.60(0.59)	0.87(0.86)

We note that the EC rates for ^{86}Kr and ^{88}Sr derived from the ground-state QRPA calculations are consistent with the one derived from the experimental data. However, the rates obtained at finite temperatures ($T = 10$ GK) are significantly larger than those obtained from the ground-state distributions stressing the importance of thermal unblocking effects in our calculation. This holds at all densities, but it is most pronounced at low densities where smaller electron energies have relatively more weight. The contribution from the GT$_+$ strength dominates the rates at lower densities (again due to the smaller electron energies involved). The contributions from forbidden multipoles becomes increasingly relevant with growing densities. At densities in excess of a few 10^{10} g cm^{-3} they dominate the rates (see also Table I). As the forbidden transitions are rather insensitive to the differences in single-particle energies obtained for the two Skyrme parametrizations and to thermal effects [35], the rates are also very similar for the two Skyrme interactions at the high densities.

Thus, the main result from Fig. 4 is that the derivation of stellar capture rates for the neutron-rich $N = 50$ nuclei on the basis of the ground state GT$_+$ distributions is unjustified. During the stellar collapse, such nuclei are quite abundant at densities of order 10^{11} g cm^{-3}. As can be read off from Fig. 4, thermal unblocking and the contributions from forbidden multipoles enhance the capture rates by an order of magnitude or more.

In Refs. [7,28,57] a hybrid model has been introduced and used to derive stellar electron-capture rates at densities in access of 10^{10} g cm^{-3}. In the first step the shell-model Monte Carlo (SMMC) method [26] is used to calculate partial occupation numbers at finite temperatures, taking multinucleon correlations into account by a residual interaction acting in large model spaces. In the second step, these partial occupation numbers serve as input into the calculation of stellar capture rates using an RPA approach. The studies within the hybrid model show that multinucleon correlations induced by the residual interaction and by thermal excitation are strong enough to overcome the shell gaps at finite temperature and to unblock the GT$_+$ strength. Figure 1 of Ref. [28] shows electron-capture rates derived within the hybrid model for selected nuclei, including ^{89}Br ($Z = 35$ and $N = 54$). The figure clearly indicates that, within the hybrid model, shell gaps, including the one at $N = 50$, are overcome at astrophysical conditions (temperatures) present during collapse at densities in access of 10^{11} g cm^{-3} (corresponding to electron chemical potentials $\mu_e > 15$ MeV [7]).

Reference [34] has performed detailed comparisons between electron-capture rates calculated for the germanium isotopes ^{76,78,80}Ge within the hybrid model and the present TQRPA approach. As can be seen in Fig. 9 of Ref. [34] there are noticeable differences between the two approaches for the conditions at low densities where details of the GT$_+$ strength distribution, induced by the different treatment of cross-shell correlations, still matter. For the reasons explained above and in Ref. [7], these differences decrease with increasing density and temperature. We also note that the capture rate decreases with increasing neutron number in the germanium isotopes. This is mainly due to the increasing Q value, which has to be overcome by the capture process, and the increasing number of neutrons partially blocking transitions into the neutron $g_{9/2}$ orbital. If we take the rates obtained at $T = 10$ GK (0.86 MeV) from Fig. 9 of Ref. [34], our present capture rate for ^{82}Ge obtained for $\rho Y_e = 10^{11}$ g cm^{-3} ($\lambda_{ec} \approx 10^3$ s^{-1}) agrees nicely with the trend of the rates for ^{76,78,80}Ge calculated with the TQRPA and the hybrid model.

In Ref. [28] a rather simple parametrization for the capture rate has been derived by fit to individual electron-capture rates available at that time (about 200 nuclei in the mass range $A = 45$–110. The purpose of the study presented in Ref. [28] was to demonstrate that the $N = 40$ shell gap does not block the GT$_+$ strength in neutron-rich nuclei and that electron capture during the later phase of the collapse proceeds on nuclei and not on free protons, as had been hypothesized earlier in the investigation of Ref. [28]. For this goal, the pool of about 200 nuclei, for which individual rates at their relevant astrophysical conditions have been evaluated and used in the supernova simulation, was sufficient. As the fit formula was rendered too simple, further individual capture rates have been derived in Ref. [7] based on a hierarchical structure approach suitable to the large set of nuclei considered. Each nucleus is described by a model which is thought to be accurate enough at the astrophysical conditions at which the nuclei contribute to the overall capture rate. The respective rate table derived by Juodagalvis and collaborators is being used in modern supernova simulation codes (see, e.g., Refs. [58,59]).

Unfortunately the rate table of Ref. [7] does not exist for individual nuclei, but rather for an ensemble of nuclei distributed in nuclear statistical equilibrium. Hence authors have recently returned to the fit formula of Ref. [28] to explore sensitivity of supernova simulations to certain input parameters [60–62]. As this formula has been derived to a pool of nuclei which does not include neutron-rich nuclei at the $N = 50$ shell gap, a comparison to the present TQRPA rates for such nuclei is quite instructive. The simple formula is based on the single-state approximation and reads [28]

$$\lambda = \frac{B \ln 2}{K}\left(\frac{T}{m_e c^2}\right)^5 [F_4(\eta) - 2\chi F_3(\eta) + \chi^2 F_2(\eta)]. \quad (6)$$

Here $K = 6146$ s, $F_k(\eta)$ are the Fermi integrals of rank k and degeneracy η, $\chi = -(Q + \Delta E)/T$,[2] and $\eta = \chi + \mu_e/T$.

---

[2]Note that, in our definition, $Q = M_f - M_i$, while in Ref. [28] the Q value is defined with opposite sign.

The fit parameters $B = 4.6$ and $\Delta E = E_f - E_i = 2.5$ MeV represent effective values for the transition strength and the energy difference between the final and initial excited states, respectively. The pool of nuclei to which the fit has been performed included pf shell nuclei and some heavier nuclei with $A < 100$. For the pf shell nuclei, which dominate the captures at lower densities $\rho < 10^{10}$ g cm^{-3}, the rates only include Gamow-Teller transitions taken from diagonalization shell-model calculations [8], while the heavier nuclei, which are relevant at densities above 10^{10} g cm^{-3} also include forbidden contributions.

In Fig. 4 we compare our TQRPA results to the fit formula. We observe that at the densities $\rho Y_e \approx 10^{11}$ g cm^{-3} where the neutron-rich $N = 50$ nuclei are relevant, the fit reproduces our TQRPA capture rates quite well. This again shows that at these late-collapse conditions the capture rates are rather insensitive to details of the nuclear response. This is not true at lower densities. For example at $\rho Y_e = 10^{10}$ g cm^{-3} the fit underestimates the TQRPA capture rates by an order of magnitude. The insufficiency of the fit under such conditions had already been discussed before (see, e.g., Ref. [60]). However, at these low densities the fit formula should not be used because the rates are still sensitive to details of the strength distributions, in particular to nuclei with rather large Q values like the neutron-rich $N = 50$ nuclei. But importantly, these nuclei are quite unabundant at these low-density conditions and hence do not contribute to the overall capture rates.

IV. CONCLUSION

We have studied the electron-capture rates on neutron-rich $N = 50$ nuclei at conditions of temperatures and densities relevant for collapse supernovae. Our calculations have been motivated by the suggestion that the $N = 50$ shell gap could serve as an obstacle for electron captures in supernovae [32,33] blocking GT$_+$ transitions. In fact, experimental GT$_+$

distributions obtained for the $N = 50$ nuclei ^{86}Kr and ^{88}Sr do not show any strength at low energies. Our $T = 0$ QRPA calculations, performed for these two nuclei and ^{78}Ni and ^{82}Ge, reproduce this observation, not showing strength at low energies $E < 7$ MeV in any of these nuclei, in agreement with Pauli blocking of the GT$_+$ strength for $N = 50$ nuclei. However, our finite-temperature TQRPA calculations also show that this blocking is overcome at finite temperatures due to thermal excitations, enabling transitions from proton $f_{7/2}$ and $g_{9/2}$ orbitals into neutron $f_{5/2}$ and $g_{7/2}$ orbitals, respectively. Both noticeably unblock the GT$_+$ strength at supernova conditions where these nuclei are abundant. Our calculations also indicate that, at the corresponding relatively-high-density conditions, forbidden transitions contribute significantly to the capture rates. The unblocking of the GT$_+$ strength at finite temperatures and the sizable forbidden contributions imply that the derivation of stellar electron-capture rates for the neutron-rich $N = 50$ nuclei on the basis of the GT$_+$ ground-state distribution, as presented in Ref. [33], is inappropriate. Our results also indicate that the neutron-rich $N = 50$ nuclei do not act as obstacles for electron captures in the later collapse phase. Our results at the relevant astrophysical conditions are in good agreement with those obtained in the hybrid model proposed in Ref. [28] which is the basis of the electron-capture rate tables [7] presently in use in supernova simulations.

ACKNOWLEDGMENTS

[1] H. A. Bethe, G. E. Brown, J. Applegate, and J. M. Lattimer, Nucl. Phys. A **324**, 487 (1979).

[2] H. A. Bethe, Rev. Mod. Phys. **62**, 801 (1990).

[3] K. Langanke and G. Martínez-Pinedo, Rev. Mod. Phys. **75**, 819 (2003).

[4] H.-T. Janka, K. Langanke, A. Marek, G. Martínez-Pinedo, and B. Müller, Phys. Rep. **442**, 38 (2007).

[5] W. Hix and F.-K. Thielemann, Astrophys. J. **460**, 869 (1996).

[6] J. Cooperstein and J. Wambach, Nucl. Phys. A **420**, 591 (1984).

[7] A. Juodagalvis, K. Langanke, W. R. Hix, G. Martínez-Pinedo, and J. M. Sampaio, Nucl. Phys. A **848**, 454 (2010).

[8] K. Langanke and G. Martínez-Pinedo, Nucl. Phys. A **673**, 481 (2000).

[9] K. Langanke and G. Martínez-Pinedo, At. Data Nucl. Data Tables **79**, 1 (2001).

[10] T. Suzuki, M. Honma, H. Mao, T. Otsuka, and T. Kajino, Phys. Rev. C **83**, 044619 (2011).

[11] Y. Fujita, B. Rubio, and W. Gelletly, Prog. Part. Nucl. Phys. **66**, 549 (2011).

[12] D. Frekers and M. Alanssari, Eur. Phys. J. A **54**, 177 (2018).

[13] E. Caurier, K. Langanke, G. Martínez-Pinedo, and F. Nowacki, Nucl. Phys. A **653**, 439 (1999).

[14] E. Caurier, G. Martínez-Pinedo, F. Nowack, A. Poves, and A. P. Zuker, Rev. Mod. Phys. **77**, 427 (2005).

[15] A. L. Cole, T. S. Anderson, R. G. T. Zegers, S. M. Austin, B. A. Brown, L. Valdez, S. Gupta, G. W. Hitt, and O. Fawwaz, Phys. Rev. C **86**, 015809 (2012).

[16] G. Fuller, W. Fowler, and M. Newman, Astrophys. J., Suppl. Ser. **48**, 279 (1982).

[17] A. Heger, K. Langanke, G. Martínez-Pinedo, and S. E. Woosley, Phys. Rev. Lett. **86**, 1678 (2001).

[18] A. Heger, S. E. Woosley, G. Martínez-Pinedo, and K. Langanke, Astrophys. J. **560**, 307 (2001).

[19] G. Fuller, W. Fowler, and M. Newman, Astrophys. J. **252**, 715 (1982).

[20] S. Bruenn, Astrophys. J., Suppl. Ser. **58**, 771 (1985).

[21] E.-W. Grewe, C. Bäumer, H. Dohmann, D. Frekers, M. N. Harakeh, S. Hollstein, H. Johansson, L. Popescu, S. Rakers, D. Savran, H. Simon, J. H. Thies, A. M. van den Berg, H. J. Wörtche, and A. Zilges, Phys. Rev. C **78**, 044301 (2008).

[22] B. P. Kay, J. P. Schiffer, S. J. Freeman, T. Adachi, J. A. Clark, C. M. Deibel, H. Fujita, Y. Fujita, P. Grabmayr, K. Hatanaka, D. Ishikawa, H. Matsubara, Y. Meada, H. Okamura, K. E. Rehm, Y. Sakemi, Y. Shimizu, H. Shimoda, K. Suda, Y. Tameshige, A. Tamii, and C. Wrede, Phys. Rev. C **79**, 021301(R) (2009).

[23] Q. Zhi, K. Langanke, G. Martínez-Pinedo, F. Nowacki, and K. Sieja, Nucl. Phys. A **859**, 172 (2011).

[24] D. J. Dean, M. T. Ressell, M. Hjorth-Jensen, S. E. Koonin, K. Langanke, and A. P. Zuker, Phys. Rev. C **59**, 2474 (1999).

[25] E. Caurier, K. Langanke, G. Martínez-Pinedo, F. Nowacki, and P. Vogel, Phys. Lett. B **522**, 240 (2001).

[26] C. W. Johnson, S. E. Koonin, G. H. Lang, and W. E. Ormand, Phys. Rev. Lett. **69**, 3157 (1992).

[27] S. Koonin, D. Dean, and K. Langanke, Phys. Rep. **278**, 1 (1997).

[28] K. Langanke, G. Martínez-Pinedo, J. M. Sampaio, D. J. Dean, W. R. Hix, O. E. Messer, A. Mezzacappa, M. Liebendörfer, H.-T. Janka, and M. Rampp, Phys. Rev. Lett. **90**, 241102 (2003).

[29] W. R. Hix, O. E. B. Messer, A. Mezzacappa, M. Liebendörfer, J. Sampaio, K. Langanke, D. J. Dean, and G. Martínez-Pinedo, Phys. Rev. Lett. **91**, 201102 (2003).

[30] C. Sullivan, E. O'Connor, R. G. T. Zegers, T. Grubb, and S. M. Austin, Astrophys. J. Lett. **816**, 44 (2016).

[31] R. Titus, C. Sullivan, R. G. T. Zegers, B. A. Brown, and B. Gao, J. Phys. G **45**, 014004 (2018).

[32] R. Titus, E. M. Ney, R. G. T. Zegers, D. Bazin, J. Belarge, P. C. Bender, B. A. Brown, C. M. Campbell, B. Elman, J. Engel, A. Gade, B. Gao, E. Kwan, S. Lipschutz, B. Longfellow, E. Lunderberg, T. Mijatovic, S. Noji, J. Pereira, J. Schmitt, C. Sullivan, D. Weisshaar, and J. C. Zamora, Phys. Rev. C **100**, 045805 (2019).

[33] J. C. Zamora, R. G. T. Zegers, S. M. Austin, D. Bazin, B. A. Brown, P. C. Bender, H. L. Crawford, J. Engel, A. Falduto, A. Gade, P. Gastis, B. Gao, T. Ginter, C. J. Guess, S. Lipschutz, B. Longfellow, A. O. Macchiavelli, K. Miki, E. Ney, S. Noji, J. Pereira, J. Schmitt, C. Sullivan, R. Titus, and D. Weisshaar, Phys. Rev. C **100**, 032801(R) (2019).

[34] A. A. Dzhioev, A. I. Vdovin, V. Y. Ponomarev, J. Wambach, K. Langanke, and G. Martínez-Pinedo, Phys. Rev. C **81**, 015804 (2010).

[35] A. A. Dzhioev, A. I. Vdovin, and C. Stoyanov, Phys. Rev. C **100**, 025801 (2019).

[36] N. Paar, G. Colò, E. Khan, and D. Vretenar, Phys. Rev. C **80**, 055801 (2009).

[37] Y. F. Niu, N. Paar, D. Vretenar, and J. Meng, Phys. Rev. C **83**, 045807 (2011).

[38] A. F. Fantina, E. Khan, G. Colò, N. Paar, and D. Vretenar, Phys. Rev. C **86**, 035805 (2012).

[39] A. A. Dzhioev, A. I. Vdovin, and C. Stoyanov, Phys. At. Nucl. **79**, 1019 (2016).

[40] J. S. O'Connell, T. W. Donnelly, and J. D. Walecka, Phys. Rev. C **6**, 719 (1972).

[41] J. D. Walecka, in *Muon Physics V2: Weak Interactions*, edited by V. W. Hughes and C. S. Wu (Elsevier Science, 1975), p. 113.

[42] A. A. Dzhioev and A. I. Vdovin, Int. J. Mod. Phys. E **18**, 1535 (2009).

[43] A. A. Dzhioev, A. I. Vdovin, V. Y. Ponomarev, and J. Wambach, Phys. At. Nucl. **72**, 1320 (2009).

[44] Y. Takahashi and H. Umezawa, Int. J. Mod. Phys. B **10**, 1755 (1996).

[45] H. Umezawa, H. Matsumoto, and M. Tachiki, *Thermofield Dynamics and Condensed States* (North-Holland, Amsterdam, 1982).

[46] J. Bartel, P. Quentin, M. Brack, C. Guet, and H.-B. Håkansson, Nucl. Phys. A **386**, 79 (1982).

[47] P.-G. Reinhard, D. J. Dean, W. Nazarewicz, J. Dobaczewski, J. A. Maruhn, and M. R. Strayer, Phys. Rev. C **60**, 014316 (1999).

[48] A. L. Goodman, Nucl. Phys. A **352**, 30 (1981).

[49] O. Civitarese, G. G. Dussel, and R. P. J. Perazzo, Nucl. Phys. A **404**, 15 (1983).

[50] N. V. Giai and H. Sagawa, Phys. Lett. B **106**, 379 (1981).

[51] N. Van Giai, C. Stoyanov, and V. V. Voronov, Phys. Rev. C **57**, 1204 (1998).

[52] J. Engel, M. Bender, J. Dobaczewski, W. Nazarewicz, and R. Surman, Phys. Rev. C **60**, 014302 (1999).

[53] J. Engel, P. Vogel, and M. R. Zirnbauer, Phys. Rev. C **37**, 731 (1988).

[54] P. Möller, A. Sierk, T. Ichikawa, and H. Sagawa, At. Data Nucl. Data Tables **109-110**, 1 (2016).

[55] E. Caurier, A. P. Zuker, A. Poves, and G. Martínez-Pinedo, Phys. Rev. C **50**, 225 (1994).

[56] K. Langanke, D. J. Dean, P. B. Radha, Y. Alhassid, and S. E. Koonin, Phys. Rev. C **52**, 718 (1995).

[57] K. Langanke, E. Kolbe, and D. J. Dean, Phys. Rev. C **63**, 032801(R) (2001).

[58] H.-T. Janka, Annu. Rev. Nucl. Part. Sci. **62**, 407 (2012).

[59] K. Kotake, T. Takiwaki, T. Fischer, K. Nakamura, and G. Martínez-Pinedo, Astrophys. J. Lett. **853**, 170 (2018).

[60] A. R. Raduta, F. Gulminelli, and M. Oertel, Phys. Rev. C **93**, 025803 (2016).

[61] A. R. Raduta, F. Gulminelli, and M. Oertel, Phys. Rev. C **95**, 025805 (2017).

[62] A. Pascal, S. Giraud, A. Fantina, F. Gulminelli, J. Novak, M. Oertel, and A. Raduta, Phys. Rev. C **101**, 015803 (2020).